Rapid Development of the Tropical Cyclone Warm Core

JONATHAN L. VIGH AND WAYNE H. SCHUBERT

Colorado State University, Fort Collins, Colorado

(Manuscript received 30 January 2009, in final form 28 April 2009)

ABSTRACT

This paper presents a simple theoretical argument to isolate the conditions under which a tropical cyclone can rapidly develop a warm-core thermal structure and subsequently approach a steady state. The theoretical argument is based on the balanced vortex model and, in particular, on the associated transverse circulation equation and the geopotential tendency equation. These second-order partial differential equations contain the diabatic forcing and three spatially varying coefficients: the static stability A, the baroclinity B, and the inertial stability C. Thus, the transverse circulation and the temperature tendency in a tropical vortex depend not only on the diabatic forcing but also on the spatial distributions of A, B, and C. Experience shows that the large radial variations of C are typically the most important effect. Under certain simplifying assumptions as to the vertical structure of the diabatic forcing and the spatial variability of A, B, and C, the transverse circulation equation and the geopotential tendency equation can be solved via separation of variables. The resulting radial structure equations retain the dynamically important radial variation of C and can be solved in terms of Green's functions. These analytical solutions show that the vortex response to a delta function in the diabatic heating depends critically on whether the heating occurs in the low-inertial-stability region outside the radius of maximum wind or in the high-inertial-stability region inside the radius of maximum wind. This result suggests that rapid intensification is favored for storms that have at least some of the eyewall convection inside the radius of maximum wind. The development of an eye partially removes diabatic heating from the high-inertial-stability region of the storm center; however, rapid intensification may continue if the eyewall heating continues to become more efficient. As the warm core matures and static stability increases over the inner core, conditions there become less favorable for deep upright convection and the storm tends to approach a steady state.

1. Introduction

One of the goals of the National Aeronautics and Space Administration's (NASA's) Tropical Cloud Systems and Processes (TCSP) research program is to understand the conditions under which a tropical cyclone can rapidly intensify (i.e., rapidly decrease its central surface pressure and rapidly increase its azimuthal wind and inner-core temperature). Understanding changes in the wind and thermal structure of a tropical cyclone is not a straightforward matter. As can be seen from (2.2) and (2.5) below, for an inviscid axisymmetric vortex the azimuthal wind tendency depends on the radial and vertical advection of angular momentum, whereas the temperature tendency depends on the diabatic heating, in addition to the radial and vertical advection terms. If the vortex is balanced (in the sense that it is continuously evolving from one gradient-balanced state to another), then the transverse circulation is determined by the solution of a second-order partial differential equation in the (r, z) plane. According to this "transverse circulation equation," first derived by Eliassen (1951) and given below in (2.11), the streamfunction for the radial and vertical motion is determined by the radial derivative of the diabatic heating and the three variable coefficients A, B, and C, which are the static stability (2.8), the baroclinity (2.9), and the inertial stability (2.10). Although solutions of (2.11) generally yield radial and vertical velocities that are much weaker than the azimuthal velocity, the radial and vertical directions are the directions of large gradients, so the relatively weak transverse circulation is crucial for vortex evolution (Ooyama 1969; Willoughby 1979). If vortex evolution is the main focus of understanding, it may be preferable to consider solutions of the geopotential tendency equation, which

Corresponding author address: Jonathan L. Vigh, Department of Atmospheric Science, Colorado State University, Fort Collins, CO 80523.
E-mail: vigh@atmos.colostate.edu

DOI: 10.1175/2009JAS3092.1

can be derived by similar means and is given below in (2.21). Note that the geopotential tendency equation is also a second-order partial differential equation with the same three variable coefficients A, B, and C.

In his classic 1951 paper, Eliassen presented the principal part of the Green's function solutions of the constant coefficient version of the transverse circulation equation for the case in which $\partial Q/\partial r$ is localized and for the case in which Q itself is localized in the (r, z) plane. These Green's function solutions clearly illustrate how the strength and shape of the transverse circulation depend on the coefficients A, B, and C. However, for applications to tropical cyclones, there are several disadvantages to Eliassen's approach: (i) the effects of top and bottom boundary conditions and the circular geometry are not included, (ii) the important spatial variability of the inertial stability coefficient C is not included, and (iii) the diabatic heating is localized in z, whereas in tropical cyclones it is rather smoothly distributed over the whole troposphere [for examples of satellite-observed vertical profiles of diabatic heating, see Fig. 6 of Rodgers et al. (1998) and Fig. 9 of Rodgers et al. (2000)]. In the present paper, we remove these limitations through a somewhat different analysis of the balanced vortex model.

We consider an idealized vortex structure and an idealized vertical structure of Q that allows the transverse circulation equation and the geopotential tendency equation to be solved by separation of variables. This leads to the radial structure Eqs. (2.24) and (2.25). Then, considering the diabatic heating as localized in r, we find the Green's functions for these ordinary differential equations, taking into account the circular geometry and the far-field boundary conditions. This simple theoretical argument isolates the conditions under which a warm-core thermal structure can rapidly develop in a tropical cyclone and thereby elaborates on the vortex heating efficiency ideas discussed in Shapiro and Willoughby (1982), Schubert and Hack (1982), Hack and Schubert (1986), and Nolan et al. (2007). The unique aspect of the present approach is its emphasis on the geopotential tendency equation as the most direct route toward understanding the rapid development of the warm core.

The paper is organized in the following way. In section 2 the balanced vortex model and the associated transverse circulation equation and geopotential tendency equation are presented, followed by a discussion of how the right-hand side of the geopotential tendency equation can be written in a compact and physically interpretable form via introduction of potential vorticity concepts, as well as a discussion of the separation of variables to reduce the partial differential equations into ordinary differential equations for the radial structure. Section 3 discusses the general solution of the radial structure problem in terms of Green's functions. The actual Green's functions are derived for a resting atmosphere in section 4 and for a Rankine-like vortex in section 5. The results of calculations from these solutions are shown in section 6 to illustrate how the temperature tendency depends on the eyewall geometry and the radial distribution of inertial stability. In section 7 we discuss observations of the radial distribution of heating and inertial stability in real storms; the implications of the impact of subsequent structure change on intensification rate are also considered. Some concluding remarks are presented in section 8.

2. Tropical cyclone theory

a. Balanced vortex model

We consider inviscid, axisymmetric, quasi-static, gradient-balanced motions of a stratified, compressible atmosphere on an f plane. As the vertical coordinate we use $z = H \ln(p_0/p)$, where $H = RT_0/g$ is the constant scale height and where p_0 and T_0 are constant reference values of pressure and temperature. We choose $p_0 =$ 100 kPa and $T_0 = 300$ K, the latter of which yields $H \approx$ 8.79 km. The governing equations for the balanced vortex model are

$$\left(f + \frac{v}{r}\right)v = \frac{\partial \phi}{\partial r}, \tag{2.1}$$

$$\frac{\partial v}{\partial t} + u\left[f + \frac{\partial (rv)}{r\partial r}\right] + w\frac{\partial v}{\partial z} = 0, \tag{2.2}$$

$$\frac{\partial \phi}{\partial z} = \frac{g}{T_0}T, \tag{2.3}$$

$$\frac{\partial (ru)}{r\partial r} + \frac{\partial (\rho w)}{\rho \partial z} = 0, \tag{2.4}$$

$$\frac{\partial T}{\partial t} + u\frac{\partial T}{\partial r} + w\left(\frac{\partial T}{\partial z} + \frac{RT}{c_p H}\right) = \frac{Q}{c_p}, \tag{2.5}$$

where u and v are the radial and azimuthal components of velocity, w is the "log-pressure vertical velocity", ϕ is the geopotential, f is the constant Coriolis parameter, c_p is the specific heat at constant pressure, $\rho(z) = \rho_0 e^{-z/H}$ is the pseudodensity, $\rho_0 = p_0/(RT_0) \approx 1.16$ kg m^{-3} is the constant reference density, and Q is the diabatic heating.

b. Transverse circulation equation

Multiplying the thermodynamic equation by g/T_0 and the tangential wind equation by $f + (2v/r)$, and then making use of the gradient and hydrostatic relations, we obtain

$$\frac{\partial \phi_t}{\partial z} + A\rho w - B\rho u = \frac{g}{c_p T_0} Q, \tag{2.6}$$

$$\frac{\partial \phi_t}{\partial r} - B\rho w + C\rho u = 0, \tag{2.7}$$

where $\phi_t = \partial\phi/\partial t$ denotes the geopotential tendency and where the static stability A, the baroclinity B, and the inertial stability C are defined by

$$\rho A = \frac{g}{T_0}\left(\frac{\partial T}{\partial z} + \frac{RT}{c_p H}\right), \tag{2.8}$$

$$\rho B = -\frac{g}{T_0}\frac{\partial T}{\partial r} = -\left(f + \frac{2v}{r}\right)\frac{\partial v}{\partial z}, \tag{2.9}$$

$$\rho C = \left(f + \frac{2v}{r}\right)\left[f + \frac{\partial (rv)}{r\partial r}\right]. \tag{2.10}$$

One way of proceeding from (2.6) and (2.7) is to eliminate ϕ_t to obtain an equation for the transverse circulation. This equation takes the form

$$\frac{\partial}{\partial r}\left[A\frac{\partial(r\psi)}{r\partial r} + B\frac{\partial \psi}{\partial z}\right] + \frac{\partial}{\partial z}\left[B\frac{\partial(r\psi)}{r\partial r} + C\frac{\partial \psi}{\partial z}\right] = \frac{g}{c_p T_0}\frac{\partial Q}{\partial r}, \tag{2.11}$$

where we have used the mass conservation principle (2.4) to express the transverse circulation in terms of ψ via the relations

$$\rho r u = -\frac{\partial(r\psi)}{\partial z} \quad \text{and} \quad \rho r w = \frac{\partial(r\psi)}{\partial r}. \tag{2.12}$$

Here we consider only vortices with $AC - B^2 > 0$ everywhere, which ensures that (2.11) is an elliptic equation. For boundary conditions on (2.11), we require that $\psi = 0$ at $z = 0$, at $z = z_T$, and at $r = 0$, and that $r\psi \to 0$ as $r \to \infty$.

c. Geopotential tendency equation

Another way of proceeding from (2.6) and (2.7) is to eliminate u and w to obtain an equation for ϕ_t. Thus, eliminating w between (2.6) and (2.7), we obtain

$$A\frac{\partial \phi_t}{\partial r} + B\frac{\partial \phi_t}{\partial z} + (AC - B^2)\rho u = \frac{g}{c_p T_0} BQ. \tag{2.13}$$

Similarly, eliminating u between (2.6) and (2.7), we obtain

$$B\frac{\partial \phi_t}{\partial r} + C\frac{\partial \phi_t}{\partial z} + (AC - B^2)\rho w = \frac{g}{c_p T_0} CQ. \tag{2.14}$$

Through the use of the mass continuity Eq. (2.4) we can now eliminate u and w between (2.13) and (2.14) to obtain

$$\frac{\partial}{r\partial r}\left(r\frac{A}{D}\frac{\partial \phi_t}{\partial r} + r\frac{B}{D}\frac{\partial \phi_t}{\partial z}\right) + \frac{\partial}{\partial z}\left(\frac{B}{D}\frac{\partial \phi_t}{\partial r} + \frac{C}{D}\frac{\partial \phi_t}{\partial z}\right) = \frac{g}{c_p T_0}\left[\frac{\partial}{r\partial r}\left(r\frac{B}{D}Q\right) + \frac{\partial}{\partial z}\left(\frac{C}{D}Q\right)\right], \tag{2.15}$$

where $D = AC - B^2$. Equation (2.15) is a second-order partial differential equation for ϕ_t, and the boundary conditions imposed on it should be consistent, via (2.6) and (2.7), with the boundary conditions for (2.11). Here we simply require that $\partial\phi_t/\partial r$ vanish at $r = 0$; that $\partial\phi_t/\partial z$ vanish at the bottom and top isobaric surfaces $z = 0$, $z = z_T$; and that $r\phi_t \to 0$ as $r \to \infty$.

We shall refer to the right-hand side of (2.15) as the "tropical cyclogenesis function" because it gives the interior forcing function associated with nonzero ϕ_t. Because of the rather complicated mathematical form given in the right-hand side of (2.15), physical interpretation is difficult. However, using potential vorticity concepts, the tropical cyclogenesis function can be transformed into a simpler form that allows straightforward physical interpretation. To accomplish this transformation, we first note that the potential vorticity equation, derived from (2.1)–(2.5), is

$$\frac{DP}{Dt} = \frac{1}{\rho}\frac{\partial(m, \dot\theta)}{r\partial(r, z)} = \frac{1}{\rho}\frac{\partial(m, \theta)}{r\partial(r, z)}\frac{\partial(m, \dot\theta)}{\partial(m, \theta)} = P\left(\frac{\partial \dot\theta}{\partial \theta}\right)_m, \tag{2.16}$$

where

$$P = \frac{1}{\rho}\frac{\partial(m, \theta)}{r\partial(r, z)} = \frac{1}{\rho}\left[-\frac{\partial v}{\partial z}\frac{\partial \theta}{\partial r} + \left(f + \frac{\partial(rv)}{r\partial r}\right)\frac{\partial \theta}{\partial z}\right] \tag{2.17}$$

is the potential vorticity, $m = rv + \frac{1}{2}fr^2$ is the absolute angular momentum per unit mass, $\theta = T(p_0/p)^\kappa$ is the potential temperature, $D/Dt = (\partial/\partial t) + u(\partial/\partial r) + w(\partial/\partial z)$ is the material derivative, $(\partial/\partial\theta)_m$ is the partial derivative with respect to θ along the absolute angular momentum surface, and $\dot\theta = Q/\Pi$, with $\Pi = c_p(p/p_0)^\kappa$ denoting the Exner function. Using (2.17) and (2.8)–(2.10), we can easily show that

$$D = AC - B^2 = \frac{g\Pi}{c_p T_0 \rho}\left(f + \frac{2v}{r}\right)P, \tag{2.18}$$

so that (2.11) and (2.15) are elliptic if $[f + (2v/r)]P > 0$. Using (2.18) we can also easily show that

$$\frac{g}{c_p T_0} r\frac{B}{D}Q = -\frac{\partial m}{\partial z}\frac{\dot\theta}{P} \quad \text{and} \quad \frac{g}{c_p T_0}\frac{C}{D}Q = \frac{\partial m}{r\partial r}\frac{\dot\theta}{P}. \tag{2.19}$$

These last two relations allow us to write

$$\frac{g}{c_p T_0}\left[\frac{\partial}{r\partial r}\left(r\frac{B}{D}Q\right)+\frac{\partial}{\partial z}\left(\frac{C}{D}Q\right)\right]=-\frac{\partial v}{\partial z}\frac{\partial(\dot\theta/P)}{\partial r}+\left[f+\frac{\partial(rv)}{r\partial r}\right]\frac{\partial(\dot\theta/P)}{\partial z}=(\boldsymbol{\zeta}\cdot\nabla)(\dot\theta/P)=\frac{\partial(m,\dot\theta/P)}{r\partial(r,z)}$$
$$=\frac{\partial(m,\theta)}{r\partial(r,z)}\frac{\partial(m,\dot\theta/P)}{\partial(m,\theta)}=\rho P\left(\frac{\partial(\dot\theta/P)}{\partial\theta}\right)_m, \tag{2.20}$$

where $\boldsymbol{\zeta}$ is the projection of the vorticity vector onto the (r, z) plane. This allows (2.15) to be rewritten as

$$\frac{\partial}{r\partial r}\left(r\frac{A}{D}\frac{\partial\phi_t}{\partial r}+r\frac{B}{D}\frac{\partial\phi_t}{\partial z}\right)+\frac{\partial}{\partial z}\left(\frac{B}{D}\frac{\partial\phi_t}{\partial r}+\frac{C}{D}\frac{\partial\phi_t}{\partial z}\right)$$
$$=\rho P\left(\frac{\partial(\dot\theta/P)}{\partial\theta}\right)_m. \tag{2.21}$$

The right-hand side of (2.21) is the compact form of the cyclogenesis function, which can now be interpreted as being proportional to the product of potential vorticity with the θ derivative of $\dot\theta/P$ along an absolute angular momentum surface. If the cyclogenesis function vanishes everywhere, we conclude from (2.21), with the aid of the boundary conditions discussed above, that $\phi_t = 0$ everywhere and the storm is in a steady state. Hausman et al. (2006) have used an axisymmetric, nonhydrostatic, full-physics model to demonstrate how a tropical cyclone approaches a steady state in which the P and $\dot\theta$ fields become locked together in a thin leaning tower on the inner edge of the eyewall cloud.

It should be noted that for the balanced vortex model, only one second-order elliptic partial differential equation needs to be solved [see Haynes and Shepherd (1989) and Wirth and Dunkerton (2006) for illustrations of this point]. Depending on the particular formulation, that elliptic equation could be the transverse circulation Eq. (2.11) or the geopotential tendency Eq. (2.21). Because our particular interest here is in the rapid development of a warm core, we find it convenient to focus much of our attention on the geopotential tendency equation.

d. Idealized vortex and the separation of variables

For real hurricanes the coefficients A, B, and C can have complicated spatial distributions [e.g., Fig. 6 of Holland and Merrill (1984) illustrates the radial and vertical variations of inertial stability and static stability computed from their composite tropical cyclone], which would preclude analytical solution of (2.11) and (2.21). To obtain analytical solutions we shall consider an idealized vortex that leads to a drastic simplification of the coefficients A and B but retains the crucial radial dependence of the inertial stability C. Thus, we consider a barotropic vortex ($B = 0$) with a static stability given by $\rho A = N^2$, where the square of the Brunt–Väisälä frequency, N^2, is a constant. The inertial stability (2.10) can then be written in the form $\rho C = \hat f^2$, where $\hat f(r) = \{[f + (2v/r)][f + \partial(rv)/r\partial r]\}^{1/2}$ is the "effective Coriolis parameter." Under the above assumptions, (2.11) reduces to

$$N^2\frac{\partial}{\partial r}\left(\frac{\partial(r\psi)}{r\partial r}\right)+\hat f^2\rho\frac{\partial}{\partial z}\left(\frac{1}{\rho}\frac{\partial\psi}{\partial z}\right)=\frac{g\rho}{c_pT_0}\frac{\partial Q}{\partial r}, \tag{2.22}$$

and (2.21) reduces to

$$N^2\frac{\partial}{r\partial r}\left(\frac{r}{\hat f^2}\frac{\partial\phi_t}{\partial r}\right)+\frac{\partial}{\rho\partial z}\left(\rho\frac{\partial\phi_t}{\partial z}\right)=\frac{g}{c_pT_0}\frac{\partial(\rho Q)}{\rho\partial z}. \tag{2.23}$$

We now assume that the diabatic heating and the streamfunction have the separable forms $e^{-z/H}Q(r,z) = \hat Q(r)\mathcal{Z}(z)$ and $\psi(r,z) = \hat\psi(r)\mathcal{Z}(z)$, where $\mathcal{Z}(z) = e^{-z/2H}\sin(\pi z/z_T)$. Because $e^{-z/H}(e^{z/H}\mathcal{Z}')' = -[(\pi/z_T)^2 + (2H)^{-2}]\mathcal{Z}$, where the prime denotes a derivative with respect to z, the partial differential Eq. (2.22) reduces to the ordinary differential equation

$$r^2\frac{d^2\hat\psi}{dr^2}+r\frac{d\hat\psi}{dr}-(\mu^2r^2+1)\hat\psi=\frac{g\rho_0r^2}{c_pT_0N^2}\frac{d\hat Q}{dr}, \tag{2.24}$$

with $\mu^2(r) = [\hat f^2(r)/N^2][(\pi/z_T)^2 + (2H)^{-2}]$ denoting the inverse Rossby length squared. The corresponding separable forms for the temperature and geopotential tendencies are $T_t(r,z) = \hat T_t(r)e^{z/H}\mathcal{Z}(z)$ and $\phi_t(r,z) = (z_T/\pi)\hat\phi_t(r)e^{z/H}\mathcal{Z}'(z)$. Because of hydrostatic balance, the radial structure functions $\hat T_t(r)$ and $\hat\phi_t(r)$ are related by $(g/T_0)\hat T_t(r) = -(z_T/\pi)[(\pi/z_T)^2 + (2H)^{-2}]\hat\phi_t(r)$. Using these results, it immediately follows that the partial differential Eq. (2.23) reduces to the ordinary differential equation

$$\hat T_t-\frac{d}{rdr}\left(\frac{r}{\mu^2}\frac{d\hat T_t}{dr}\right)=\frac{\hat Q}{c_p}. \tag{2.25}$$

Note that although it has a certain resemblance to the thermodynamic equation, (2.25) follows directly from (2.21), which has been obtained through a combination of all the original Eqs. (2.1)–(2.5). The remainder of this paper deals with the physical insights revealed by analytical solutions of (2.24) and (2.25). As is easily shown

by integration of (2.25) and use of the boundary conditions, these solutions have the integral property

$$\int_0^\infty \hat{T}_t r\, dr = \int_0^\infty \frac{\hat{Q}}{c_p} r\, dr, \tag{2.26}$$

so the integrated local temperature change is equal to the integrated diabatic heating. However, the crucial question for hurricane intensification is whether the local temperature change occurs primarily in the region of diabatic heating or is spread over a much larger region. This question can be answered by examining the solutions of (2.25), which show the following general properties. If the diabatic heating $\hat{Q}/c_p$ is localized to a region of large Rossby length (i.e., a region where μ^{-2} is large), then $d^2\hat{T}_t/dr^2$ tends to be small, so that $\hat{T}_t$ tends to be spread over a large area but with values much smaller than the peak value of $\hat{Q}/c_p$. In contrast, if the diabatic heating occurs in a region of small Rossby length (i.e., a region where μ^{-2} is small), then $d^2\hat{T}_t/dr^2$ tends to be larger, so that $\hat{T}_t$ tends to be confined to a smaller area, with values more comparable to the peak value of $\hat{Q}/c_p$. The former case tends to occur when a vortex is weak—that is, when the effective Coriolis parameter $\hat{f}(r)$ is small and the Rossby length $\mu^{-1}(r)$ is large. However, as the vortex becomes stronger, $\hat{f}(r)$ becomes larger and $\mu^{-1}(r)$ becomes smaller, so that the diabatic heating results in a tendency $\hat{T}_t(r)$ that is more localized to the region where $\hat{Q}(r)$ is confined. This process can result in the rapid development of a tropical cyclone warm core. In the following sections we attempt to provide a more quantitative understanding of these simple qualitative arguments.

3. General solution in terms of the Green's function

The solution of (2.25) can be written in the form

$$\hat{T}_t(r) = \int_0^\infty G(r, r')\frac{\hat{Q}(r')}{c_p} r'\, dr', \tag{3.1}$$

where the Green's function $G(r, r')$ satisfies the differential equation

$$G(r, r') - \frac{d}{rdr}\left[\frac{r}{\mu^2}\frac{dG(r, r')}{dr}\right] = \frac{\delta(r - r')}{r'}, \tag{3.2}$$

with $\delta(r - r')$ denoting the Dirac delta function localized at radius r'. The validity of (3.1) and (3.2) can easily be confirmed by substituting (3.1) into (2.25) and noting that $\int_0^\infty \hat{Q}(r')\,\delta(r - r')\, dr' = \hat{Q}(r)$. The Green's function $G(r, r')$ gives the radial distribution of the temperature tendency when the diabatic heating is confined to a very narrow region at radius r'. It satisfies the boundary conditions

$$\frac{dG(r, r')}{dr} = 0 \quad \text{at} \quad r = 0, \quad rG(r, r') \to 0 \quad \text{as} \quad r \to \infty \tag{3.3}$$

and the jump conditions

$$[G(r, r')]_{r=r'-}^{r=r'+} = 0 \quad \text{and} \quad \left[\frac{r}{\mu^2}\frac{dG(r, r')}{dr}\right]_{r=r'-}^{r=r'+} = -1, \tag{3.4}$$

the latter of which is derived by integrating (3.2) across a narrow interval centered at radius r'.

The solution of (2.24) could be obtained in an analogous way. However, it is simpler to determine $G_\psi(r, r')$, the Green's function for ψ, directly from $G(r, r')$, the Green's function for the temperature tendency. This can be accomplished by noting that the thermodynamic Eq. (2.6), with the assumptions given in section 2, leads to

$$\frac{d[rG_\psi(r, r')]}{rdr} = -\frac{g\rho_0}{T_0 N^2} G(r, r') \quad \text{for} \quad r \neq r'. \tag{3.5}$$

Thus, once we have determined $G(r, r')$, we can obtain $G_\psi(r, r')$ by integration of (3.5).

The differential Eq. (3.2) for the Green's function $G(r, r')$ can be solved analytically only if $\mu(r)$ takes some simple form. Here we present two simple cases. In the first case (section 4) the atmosphere is assumed to be at rest, so that μ is a constant. In the second case (section 5) we consider a Rankine-like vortex, so that μ is piecewise constant, with a large value of μ in the vortex core and a small value of μ in the far field.

4. Green's functions for a resting atmosphere

We first consider the case where $v = 0$, so that $\hat{f}(r) = f$ and $\mu(r)$ takes on the constant value μ_f. Then, (3.2) reduces to the order zero modified Bessel equation (Abramowitz and Stegun 2006, chapter 9) when $r \neq r'$. The general solution of the problem is constructed from a combination of the order zero modified Bessel functions $I_0(\mu_f r)$ and $K_0(\mu_f r)$. Because of the boundary conditions (3.3), only the $I_0(\mu_f r)$ solution is valid for $r < r'$ and only the $K_0(\mu_f r)$ solution is valid for $r > r'$. Matching these solutions across $r = r'$ involves the jump conditions (3.4), which can be enforced with the aid of the derivative relations $dI_0(x)/dx = I_1(x)$ and $dK_0(x)/dx = -K_1(x)$ and the Wronskian $I_0(x)K_1(x) + K_0(x)I_1(x) = 1/x$. The final result is

$$G(r, r') = \mu_f^2 \begin{cases} K_0(\mu_f r') I_0(\mu_f r) & \text{if} \quad 0 \le r \le r' \\ I_0(\mu_f r') K_0(\mu_f r) & \text{if} \quad r' \le r < \infty. \end{cases} \tag{4.1}$$

Integrating (3.5), using (4.1) and the derivative relations $d[rI_1(\mu r)]/rdr = \mu I_0(\mu r)$ and $d[rK_1(\mu r)]/rdr = -\mu K_0(\mu r)$, we obtain

$$G_\psi(r, r') = \frac{g\rho_0\mu_f}{T_0 N^2} \begin{cases} -K_0(\mu_f r') I_1(\mu_f r) & \text{if} \quad 0 \le r < r' \\ I_0(\mu_f r') K_1(\mu_f r) & \text{if} \quad r' < r < \infty. \end{cases} \tag{4.2}$$

To compute the actual temperature tendency associated with the Green's function (4.1), we return to (3.1) with the condition $\hat{Q}(r') = 0$ for $r' \neq r_h$. Then (3.1) becomes

$$\hat{T}_t(r) = G(r, r_h) \int_{r_h-}^{r_h+} \frac{\hat{Q}(r')}{c_p} r' \, dr'. \tag{4.3}$$

Note that according to (4.3), the spatial distribution of $\hat{T}_t(r)$ is given by $G(r, r_h)$ and the magnitude by $\int_{r_h-}^{r_h+} [\hat{Q}(r')/c_p] r' \, dr'$, which is somewhat arbitrary. We have chosen this normalization factor to be

$$\int_{r_h-}^{r_h+} \frac{\hat{Q}(r')}{c_p} r' \, dr' = (26 \, \mathrm{K \, h^{-1}})(25 \, \mathrm{km})(10 \, \mathrm{km}) \equiv S, \tag{4.4}$$

which is the same normalization used by Schubert et al. (2007) in their study of the distribution of subsidence in the hurricane eye. With this normalization, the $\psi(r, z)$ and $T_t(r, z)$ fields can be written as

$$\psi(r, z) = S G_\psi(r, r_h) e^{-z/(2H)} \sin\left(\frac{\pi z}{z_T}\right), \tag{4.5}$$

$$T_t(r, z) = S G(r, r_h) e^{z/(2H)} \sin\left(\frac{\pi z}{z_T}\right). \tag{4.6}$$

Figure 1 shows contours of $r\psi$ and T_t in the (r, z) plane for this resting atmosphere case. These plots have been constructed from (4.5) and (4.6) using the Green's function Eqs. (4.1) and (4.2). Note that $r\psi$ is negative for $r <$ 25 km and positive for $r >$ 25 km, which means that the transverse mass flux is counterclockwise for $r <$ 25 km and clockwise for $r >$ 25 km. The discontinuity of $r\psi$ at $r =$ 25 km means that infinite upward vertical velocity occurs there. However, the vertical mass flux is finite because

$$\rho \int_{r_h-}^{r_h+} w(r, z) r \, dr = r_h[\psi(r_h+, z) - \psi(r_h-, z)] = \frac{g\rho_0 S}{T_0 N^2} e^{-z/(2H)} \sin\left(\frac{\pi z}{z_T}\right), \tag{4.7}$$

which follows from (4.2), (4.5), and the Wronskian. The minimum value of $r\psi$, which occurs just inside $r =$ 25 km, is given in the sixth column of the first row in Table 1, while the maximum value of $r\psi$, which occurs just outside $r =$ 25 km, is given in the seventh column. Thus, at the level of maximum vertical mass fluxes, the downward mass flux inside $r =$ 25 km is 0.5339×10^6 kg s^{-1}, while the downward mass flux outside $r =$ 25 km is 448.38×10^6 kg s^{-1}. Defining $\eta = (r\psi)_{\max}/[(r\psi)_{\max} - (r\psi)_{\min}]$ as the fraction of the upward mass flux that is compensated by far-field subsidence, we see (eighth column of Table 1) that approximately 99.88% of the upward mass flux is compensated by downward mass flux outside $r =$ 25 km and only 0.12% is compensated by downward mass flux inside $r =$ 25 km. As can be seen in the right panel of Fig. 1, there is very little variation of the temperature tendency on a fixed isobaric surface. In other words, the Dirac delta function in the diabatic heating leads to a transverse circulation that raises the temperature on a given isobaric surface nearly uniformly over a large area. The production of very weak horizontal temperature gradients and corresponding weak vertical shears of the azimuthal wind is consistent with the well-known result that diabatic heating on a horizontal scale smaller than the Rossby length is a very inefficient way to produce rotational flow (e.g., Schubert et al. 1980; Gill 1982; Shapiro and Willoughby 1982; Schubert and Hack 1982).

Although the assumption of a resting atmosphere is too restrictive for our present goals, the idealized Green's functions (4.1) and (4.2) provide useful comparisons for the more general results of section 5.

5. Green's functions for a nonresting atmosphere

a. A Rankine-like vortex

To treat radial variations of $\mu(r)$ in a simple manner, we consider the specific barotropic vortex in which the square of the absolute angular momentum is given by $m^2(r) = [rv(r) + \frac{1}{2} f r^2]^2 = \frac{1}{4} f_c^2 r^4$ for $0 \le r \le r_c$ and by $m^2(r) = m^2(r_c) + \frac{1}{4} f^2 (r^4 - r_c^4)$ for $r_c \le r < \infty$, where r_c and f_c are specified constants giving the radius and strength of the vortex core. It can easily be shown that

$$\hat{f}(r) = \left(\frac{\partial m^2}{r^3 \partial r}\right)^{1/2} = \left[\left(f + \frac{2v}{r}\right)\left(f + \frac{\partial (rv)}{r \partial r}\right)\right]^{1/2} = \begin{cases} f_c, & \text{if} \quad 0 \le r < r_c \ \text{(vortex core)}, \\ f, & \text{if} \quad r_c < r < \infty \ \text{(far field)}, \end{cases} \tag{5.1}$$

so that f_c can be interpreted as a specified constant giving the effective Coriolis parameter in the vortex core. Because of (5.1), the inverse Rossby length $\mu(r)$ also has the piecewise constant form

$$\mu(r) = \begin{cases} \mu_c & \text{if} \quad 0 \le r < r_c \ \text{(vortex core)}, \\ \mu_f & \text{if} \quad r_c < r < \infty \ \text{(far field)}, \end{cases} \tag{5.2}$$

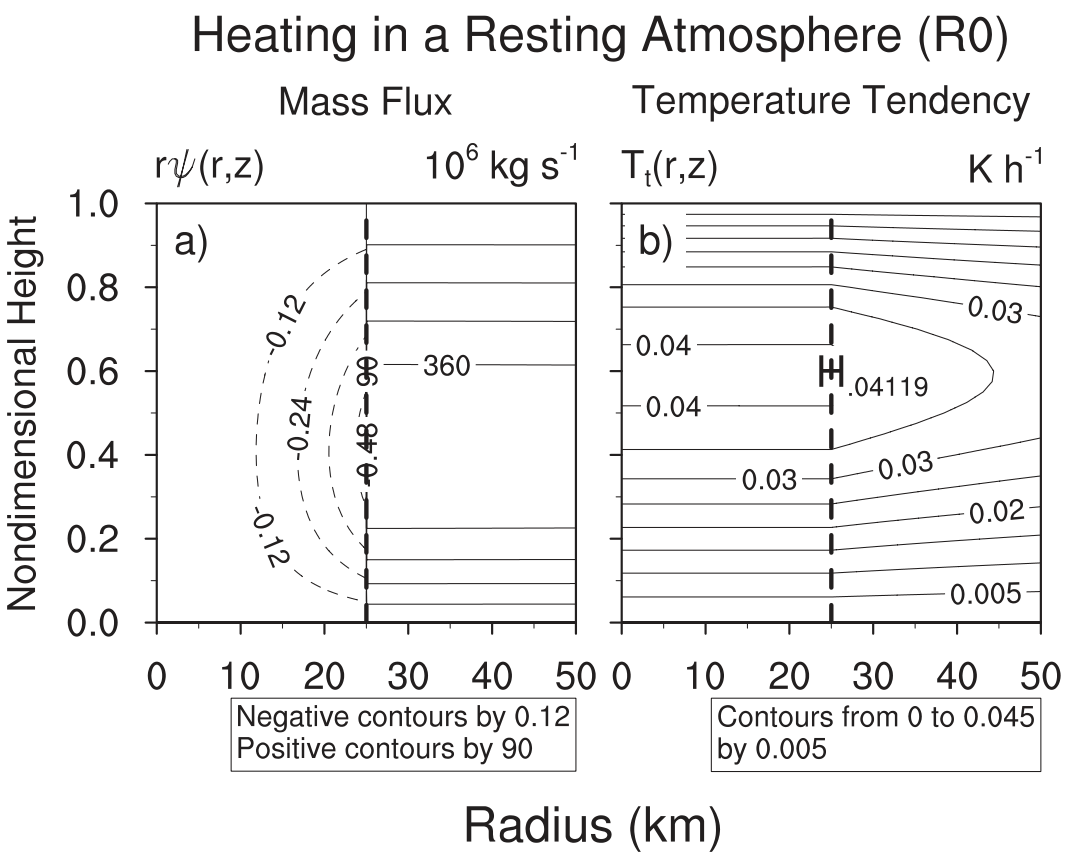

FIG. 1. Isolines of $r\psi$ and temperature tendency T_t in the (r, z) plane for the resting atmosphere case. The radial axis is labeled in km and the vertical axis in the dimensionless vertical coordinate z/z_T. The radius of diabatic heating is $r_h = 25$ km (as indicated by the vertical dashed line).

where the constants μ_c and μ_f are defined in terms of the constants f_c and f via $\mu_c = (f_c/N)[(\pi/z_T)^2 + (2H)^{-2}]^{1/2}$ and $\mu_f = (f/N)[(\pi/z_T)^2 + (2H)^{-2}]^{1/2}$. Plots of $v(r)$, computed using the parameters listed in the second (sixth) through the fifth (ninth) rows of Table 1, are shown in the left column of Fig. 2 (Fig. 3). In constructing Table 1 and Figs. 2 and 3, we have used $f = 5 \times 10^{-5}$ s^{-1} and $\mu_f^{-1} = 1000$ km. Note that the $v(r)$ profiles are Rankine-like and that the strength of the tangential winds range from tropical depression, through tropical storm, to Category 1 on the Saffir–Simpson scale. The Rossby length in the vortex core, given by μ_c^{-1} and listed in the fifth column of Table 1, is less than 20 km for the stronger vortices.

TABLE 1. Parameters for the resting case (first row) and the Rankine-like vortex cases (remaining rows): radius of the vortex core, r_c; maximum azimuthal wind, $v(r_c)$; dimensionless effective Coriolis parameter in the vortex core, f_c/f; and Rossby length in the vortex core, μ_c^{-1}. The last four columns show the minimum value of $r\psi$ (which occurs just inside $r = r_h$), the maximum value of $r\psi$ (just outside $r = r_h$), the fraction (η) of the downward mass flux that occurs in the region $r > r_h$, and the maximum value of T_t.

Case	r_c (km)	$v(r_c)$ (m s^{-1})	f_c/f	μ_c^{-1} (km)	$(r\psi)_{\min}$ ($\times 10^6$ kg s^{-1})	$(r\psi)_{\max}$ ($\times 10^6$ kg s^{-1})	η (%)	$(T_t)_{\max}$ (K h^{-1})
R0	—	0	1.0	1000.0	−0.5339	448.38	99.88	0.0411946
A10	20	10	21.0	47.6	−0.5266	448.39	99.88	0.0411952
A20	20	20	41.0	24.4	−0.5081	448.41	99.89	0.0411969
A30	20	30	61.0	16.4	−0.4830	448.44	99.89	0.0411992
A40	20	40	81.0	12.3	−0.4557	448.46	99.90	0.0412018
B10	30	10	14.3	69.8	−5.5922	443.31	98.75	0.43832
B20	30	20	27.7	36.1	−18.099	430.75	95.97	1.47819
B30	30	30	41.0	24.4	−35.154	413.61	92.17	3.05366
B40	30	40	54.3	18.4	−53.852	394.81	88.00	5.04679

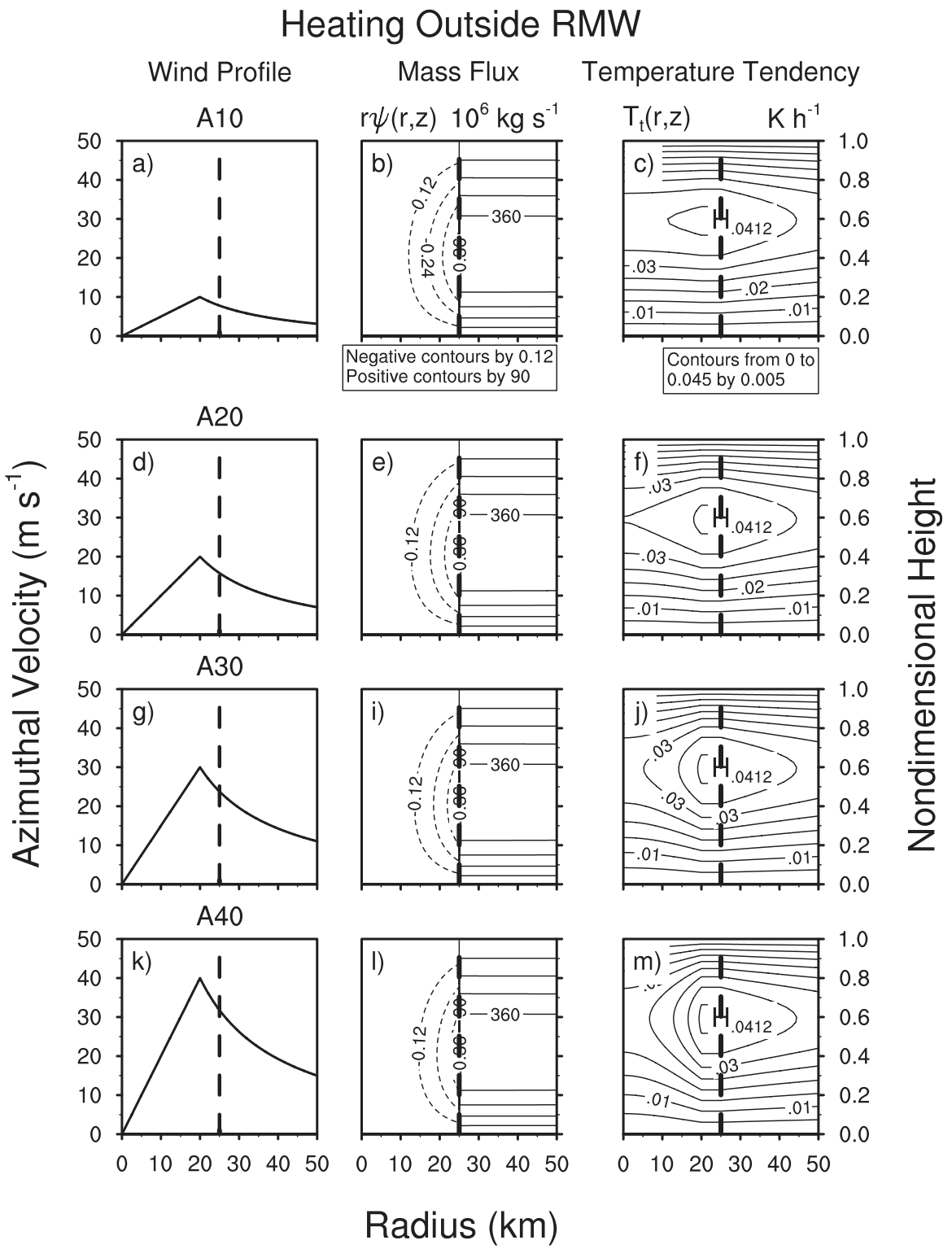

FIG. 2. Isolines of $r\psi(r, z)$ and temperature tendency $T_t(r, z)$ for the four Rankine-like vortices shown in the left column. The radius of maximum wind is $r_c = 20$ km and the radius of diabatic heating is $r_h = 25$ km (as indicated by the vertical dashed line).

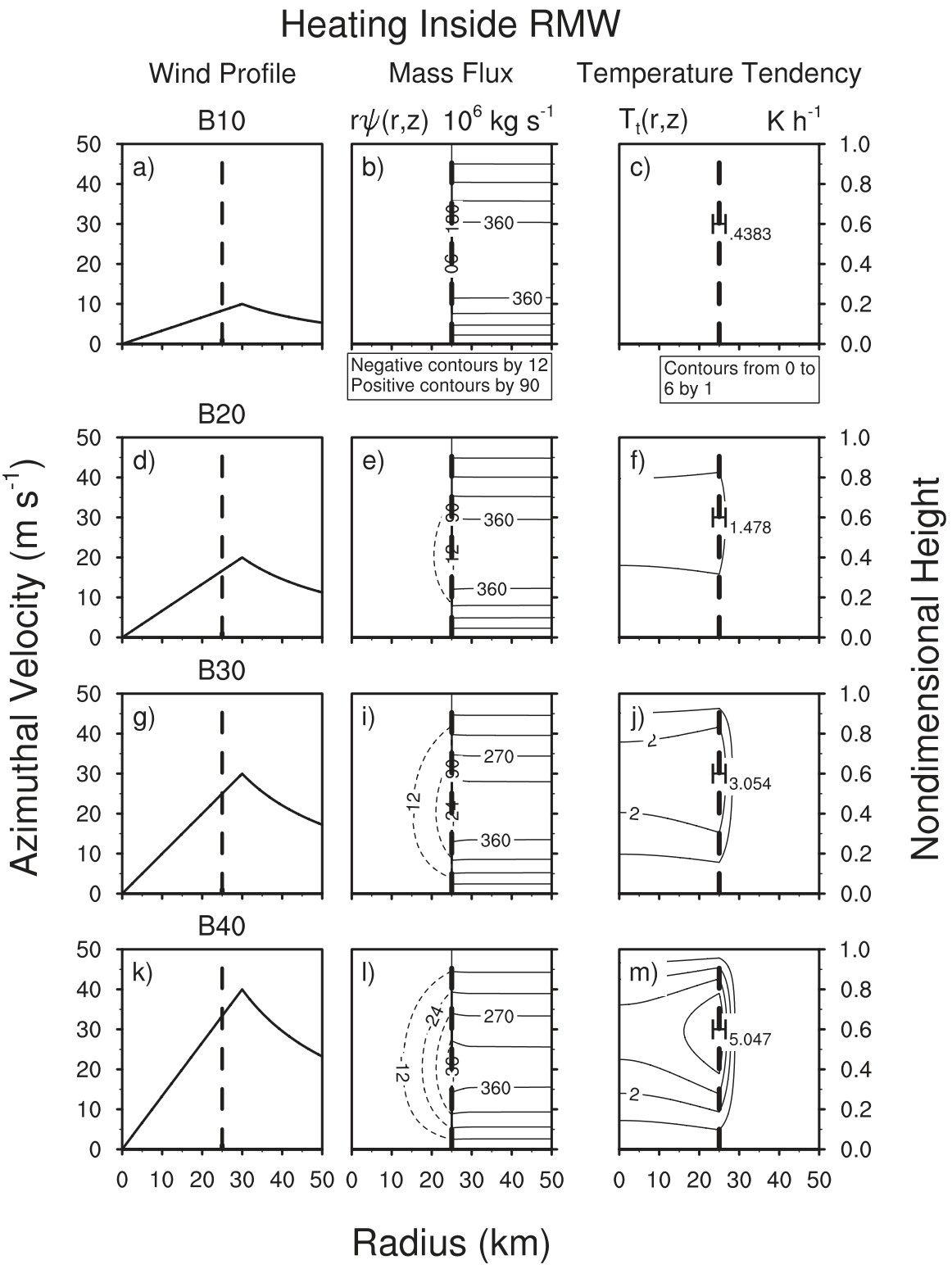

FIG. 3. As in Fig. 2, but for r_c = 30 km, so the diabatic heating occurs inside the radius of maximum wind. Note the change in isoline intervals from those used in Fig. 2.

b. Diabatic heating outside the vortex core ($r_c < r_h$)

To solve the Green's function problem (3.2)–(3.4) for this Rankine-like vortex, we first consider the case $r_c < r_h$. Then (3.2) reduces to

$$\frac{d}{rdr}\left[r\frac{dG(r, r_h)}{dr}\right] - \mu_c^2 G(r, r_h) = 0 \quad \text{if} \quad 0 \le r < r_c,$$

$$\frac{d}{rdr}\left[r\frac{dG(r, r_h)}{dr}\right] - \mu_f^2 G(r, r_h) = 0 \quad \text{if} \quad r_c < r < \infty \quad \text{but} \quad r \ne r_h. \tag{5.3}$$

Now, in addition to the boundary conditions (3.3) and the jump conditions (3.4), we require

$$[G(r, r_h)]_{r=r_c-}^{r=r_c+} = 0 \quad \text{and} \quad \left[\frac{r}{\mu^2}\frac{dG(r, r_h)}{dr}\right]_{r=r_c-}^{r=r_c+} = 0, \tag{5.4}$$

the latter of which is derived by integrating (3.2) across a narrow interval centered at $r = r_c$. The solution of (5.3) consists of linear combinations of the zeroth-order modified Bessel functions $I_0(\mu_c r)$ and $K_0(\mu_c r)$ in the region $0 \le r < r_c$ and linear combinations of $I_0(\mu_f r)$ and $K_0(\mu_f r)$ in the region $r_c < r < \infty$. Because our boundary condition requires that $dG(r, r_h)/dr = 0$ at $r = 0$, we can discard the $K_0(\mu_c r)$ solution in the inner region. Similarly, because $rG(r, r_h) \to 0$ as $r \to \infty$, we can discard the $I_0(\mu_f r)$ solution in the outer region. The solution of (5.3) can then be written as

$$G(r, r_h) = \mu_f^2 \begin{cases} F_1(r_c, r_h)K_0(\mu_f r_h)I_0(\mu_c r) & 0 \le r \le r_c \\ F_1(r, r_h)K_0(\mu_f r_h)I_0(\mu_c r_c) + \gamma_1 F_1(r_c, r)I_0(\mu_f r_h)K_0(\mu_f r_h) & r_c \le r \le r_h \\ \gamma_1 F_1(r_c, r_h)I_0(\mu_f r_h)K_0(\mu_f r) & r_h \le r < \infty, \end{cases} \tag{5.5}$$

where

$$F_1(x, y) = \frac{I_0(\mu_f x)K_0(\mu_f y) - K_0(\mu_f x)I_0(\mu_f y)}{I_0(\mu_c r_c)K_0(\mu_f r_h) - \gamma_1 K_0(\mu_f r_c)I_0(\mu_f r_h)} \tag{5.6}$$

and

$$\gamma_1 = \mu_f r_c\left[I_0(\mu_c r_c)K_1(\mu_f r_c) + \frac{\mu_f}{\mu_c}I_1(\mu_c r_c)K_0(\mu_f r_c)\right] + \mu_f r_c\left[I_0(\mu_c r_c)I_1(\mu_f r_c) - \frac{\mu_f}{\mu_c}I_1(\mu_c r_c)I_0(\mu_f r_c)\right]\frac{K_0(\mu_f r_h)}{I_0(\mu_f r_h)}. \tag{5.7}$$

Since $F_1(r_c, r_c) = 0$ and $F_1(r_h, r_h) = 0$, (5.5) guarantees that $G(r, r_h)$ is continuous at $r = r_c$ and $r = r_h$, so that the first entry in (3.4) and the first entry in (5.4) are both satisfied. The jump condition on the derivative at $r = r_h$ [i.e., the second entry in (3.4)] and the jump condition on the derivative at $r = r_c$ [i.e., the second entry in (5.4)] can be confirmed by using the Bessel function derivative relations and the Wronskian. The Green's function for ψ can be obtained by integrating (3.5), using (5.5) for $G(r, r_h)$. The result is

$$G_\psi(r, r_h) = \frac{g\rho_0\mu_f}{T_0 N^2} \begin{cases} -\dfrac{\mu_f}{\mu_c}F_1(r_c, r_h)K_0(\mu_f r_h)I_1(\mu_c r) & 0 \le r \le r_c \\ -K_0(\mu_f r_h)[I_0(\mu_c r_c)\hat{F}_1(r_h, r) - \gamma_1 I_0(\mu_f r_h)\hat{F}_1(r_c, r)] & r_c \le r < r_h \\ \gamma_1 F_1(r_c, r_h)I_0(\mu_f r_h)K_1(\mu_f r) & r_h < r < \infty, \end{cases} \tag{5.8}$$

where

$$\hat{F}_1(x, y) = \frac{K_0(\mu_f x)I_1(\mu_f y) + I_0(\mu_f x)K_1(\mu_f y)}{I_0(\mu_c r_c)K_0(\mu_f r_h) - \gamma_1 K_0(\mu_f r_c)I_0(\mu_f r_h)}. \tag{5.9}$$

To summarize for the case $r_c < r_h$, after specifying μ_c, μ_f, r_c, and r_h, we can compute γ_1 from (5.7), and then $G(r, r_h)$ from (5.5) and $G_\psi(r, r_h)$ from (5.8). Note that when $\mu_c = \mu_f$, (5.7) reduces to $\gamma_1 = 1$, the first two lines of (5.5) become identical, the first two lines of (5.8)

become identical, and (5.5) reduces to (4.1) while (5.8) reduces to (4.2).

c. Diabatic heating within the vortex core ($r_h < r_c$)

Now consider the case $r_h < r_c$. The Green's function for the temperature tendency is

$$G(r, r_h) = \mu_c^2 \begin{cases} \gamma_2 F_2(r_h, r_c) K_0(\mu_c r_h) I_0(\mu_c r) & 0 \le r \le r_h \\ \gamma_2 F_2(r, r_c) K_0(\mu_c r_h) I_0(\mu_c r_h) + F_2(r_h, r) I_0(\mu_c r_h) K_0(\mu_f r_c) & r_h \le r \le r_c \\ F_2(r_h, r_c) I_0(\mu_c r_h) K_0(\mu_f r) & r_c \le r < \infty, \end{cases} \tag{5.10}$$

where

$$F_2(x, y) = \frac{I_0(\mu_c x) K_0(\mu_c y) - K_0(\mu_c x) I_0(\mu_c y)}{I_0(\mu_c r_h) K_0(\mu_f r_c) - \gamma_2 K_0(\mu_c r_h) I_0(\mu_c r_c)} \tag{5.11}$$

and

$$\gamma_2 = \mu_c r_c \left[K_0(\mu_f r_c) I_1(\mu_c r_c) + \frac{\mu_c}{\mu_f} I_0(\mu_c r_c) K_1(\mu_f r_c) \right] + \mu_c r_c \left[K_0(\mu_f r_c) K_1(\mu_c r_c) - \frac{\mu_c}{\mu_f} K_0(\mu_c r_c) K_1(\mu_f r_c) \right] \frac{I_0(\mu_c r_h)}{K_0(\mu_c r_h)}. \tag{5.12}$$

Note that the continuity of $G(r, r_h)$ at $r = r_h$ and $r = r_c$ follows directly from $F_2(r_h, r_h) = 0$ and $F_2(r_c, r_c) = 0$. The Green's function for ψ is

$$G_\psi(r, r_h) = \frac{g\rho_0\mu_c}{T_0 N^2} \begin{cases} -\gamma_2 F_2(r_h, r_c) K_0(\mu_c r_h) I_1(\mu_c r) & 0 \le r < r_h \\ I_0(\mu_c r_h)[-\gamma_2 K_0(\mu_c r_h) \hat{F}_2(r_c, r) + K_0(\mu_f r_c) \hat{F}_2(r_h, r)] & r_h < r \le r_c \\ \dfrac{\mu_c}{\mu_f} F_2(r_h, r_c) I_0(\mu_c r_h) K_1(\mu_f r) & r_c \le r < \infty, \end{cases} \tag{5.13}$$

where

$$\hat{F}_2(x, y) = \frac{K_0(\mu_c x) I_1(\mu_c y) + I_0(\mu_c x) K_1(\mu_c y)}{I_0(\mu_c r_h) K_0(\mu_f r_c) - \gamma_2 K_0(\mu_c r_h) I_0(\mu_c r_c)}. \tag{5.14}$$

When $\mu_c = \mu_f$, (5.12) reduces to $\gamma_2 = 1$, the last two lines of (5.10) become identical, the last two lines of (5.13) become identical, and (5.10) reduces to (4.1) while (5.13) reduces to (4.2).

6. Conditions for rapid development of a warm core

a. Inner-core response to heating

Plots of mass streamfunction $r\psi(r, z)$ and temperature tendency $T_t(r, z)$ can now be constructed from (4.5) and (4.6) using either (5.5) and (5.8) for $r_c < r_h$ or (5.10) and (5.13) for $r_h < r_c$. It can be shown that the $r\psi(r, z)$ field constructed in this way also satisfies the mass flux normalization relation (4.7).

We first consider the case $r_c = 20$ km and $r_h = 25$ km, which is typical of cases in which the diabatic heating lies outside the radius of maximum wind. In the second and third columns of Fig. 2 we show isolines of $r\psi(r, z)$ and $T_t(r, z)$ for the four vortices displayed in the left column. These vortices all have a maximum wind at $r_c = 20$ km, but with $v(r_c) = 10$, 20, 30, and 40 m s^{-1}. The corresponding values of f_c/f and μ_c^{-1} are given in the fourth and fifth columns of Table 1, along the rows labeled A10, A20, A30, and A40. The most obvious feature of Fig. 2 is the similarity of the four $r\psi(r, z)$ fields and the four $T_t(r, z)$ fields, together with the fact that they differ little from the resting case shown in Fig. 1. For example, the peak value of $T_t(r, z)$ is 0.041 195 K h^{-1} for case A10 and 0.041 202 K h^{-1} for case A40. Because the vortex core is more inertially stable in case A40, the compensating subsidence does not extend as far inward, which means the subsidence is not as large at $r = 0$ and thus T_t is not as large at $r = 0$. This explains why the temperature tendency in Fig. 2m is somewhat more localized than the temperature tendency in Fig. 2c. This ''warm-ring effect'' has been observed in real storms such as Hurricane Isabel (2003; see Fig. 10 of Schubert et al. 2007). However, the main conclusion to be drawn from Fig. 2 is that diabatic

heating in the low-inertial-stability region outside the radius of maximum wind produces a temperature tendency that is nearly uniform horizontally and similar to that found for a resting atmosphere. In other words, diabatic heating outside the radius of maximum wind is very inefficient at producing rotational flow, no matter how small the Rossby length inside the radius of maximum wind.

Now consider the case $r_h = 25$ km and $r_c = 30$ km, which is typical of cases in which the diabatic heating lies inside the radius of maximum wind. In the second and third columns of Fig. 3 we show isolines of $r\psi(r, z)$ and $T_t(r, z)$ for the four vortices displayed in the left column. These vortices all have a maximum wind at $r_c = 30$ km, but with $v(r_c) = 10$, 20, 30, and 40 m s^{-1}. The corresponding values of f_c/f and μ_c^{-1} are given in the fourth and fifth columns of Table 1, along the rows labeled B10, B20, B30, and B40. The most obvious features of Fig. 3 are the much larger and more localized values of $T_t(r, z)$ near $r = 25$ km. The values are approximately 10 (0.4383 K h^{-1} for case B10) to 100 (5.047 K h^{-1} for case B40) times the values in Fig. 2. *Thus, when diabatic heating occurs within the high-inertial-stability region that lies inside the radius of maximum wind, there is enhanced subsidence inside the radius of heating*[1] *and a tendency to rapidly form a warm core.*

It should be noted that while all results shown here represent the heating as a Dirac delta function, these results could be extended for a more general distribution of heating of finite width. Because of the linearity of the geopotential tendency equation and the transverse circulation equation, we can construct solutions for general diabatic heating fields by superposition of the Green's functions $G(r, r')$ and $G_\psi(r, r')$ for different values of r'. This allows us to argue as follows: Suppose that the diabatic heating field consists of an annular ring of finite width and that the radius of maximum wind occurs somewhere between the inner and outer edges of this ring. In this case, the portion of the diabatic heating that occurs inside the radius of maximum wind contributes much more efficiently to warm core formation and vortex intensification than the portion of the diabatic heating that occurs outside the radius of maximum wind. A consequence is that the inward or outward movement of the radius of maximum wind relative to the annular ring of convection can have a large effect on the vortex intensification rate.

b. Outer core response to heating

Further physical insight may be gained by noting subtle differences among Figs. 1, 2, and 3. Isolines of $r\psi(r, z)$ for the B40 vortex in Fig. 3l possess a discernible slope between r_h and r_c, whereas they do not in Figs. 1 and 2l. This slope indicates that significant subsidence (and therefore adiabatic warming) occurs locally outside of the diabatic forcing region where the inertial stability remains high. As a word of caution, it should be recognized that our idealized vortex has a very large change of inertial stability at the radius of maximum winds and thereby accentuates the difference between the efficiency of diabatic heating just inside and just outside this radius. In real hurricanes the variation of inertial stability with radius (Mallen et al. 2005; Holland and Merrill 1984) is somewhat smoother, so there is a more gradual change from the inefficient response to diabatic heating outside the radius of maximum wind to the efficient response inside this radius. In Holland and Merrill's composite tropical cyclone, inertial stability peaks at approximately $1000f^2$ at $r \approx 30$ km, decreases rapidly to $100f^2$ at $r \approx 80$ km, and then drops off more gradually to $10f^2$ at $r \approx 200$ km. The corresponding Rossby length at $r \approx 200$ km is approximately 300 km, or one-third that of the far-field value (1000 km), so the heating there will still be considerably more efficient than in the far field. Thus, heating in this transition region can still spin up the local tangential wind and radially constrain the circulation response—despite the fact that the heating is occurring outside of the radius of maximum wind. This causes strong subsidence warming and increased static stability outside of the inner core, which will tend to inhibit convection. According to the authors, this effect likely explains the relatively clear doughnut-shaped region sometimes observed surrounding intense storms following a period of rapid intensification.[2] Annular hurricanes have been noted to lack significant outer rainbands (Knaff et al. 2003) and may also possess a vortex "skirt" outside of the radius of maximum winds. Our simple analytic results suggest that the enhanced outer subsidence associated with such a vortex skirt may be implicated in suppressing these outer rainbands. This effect has also been suggested by a recent full-physics modeling study by Wang (2008).

c. Far-field response to heating

In passing, we note that the outer core ($r \approx 50$ km) temperature tendencies are qualitatively similar between all three figures,[3] but the far-field tendencies (e.g., $r \sim 500$ km, not shown) of Fig. 3 are slightly less than the

[1] See the values of η listed in Table 1. Smaller η values indicate that more of the mass flux recirculates into the eye.

[2] For an example, see the remarkable clear "moat" that surrounded Hurricane Allen (1980) shown in Fig. 1e of Jorgensen (1984).

[3] This difference is not very apparent from the figures because the isoline levels have been changed in Fig. 3 to highlight the enhanced inner-core tendency response.

tendencies in Figs. 1 and 2. This difference is easily explained by recalling from (2.26) that the integrated local temperature tendency must be equal to the integrated diabatic heating. So in Fig. 3, the large temperature tendencies of the small inner-core region are exactly compensated for by the slightly reduced tendencies (compared to Figs. 1 and 2) over the expansive far-field region.

7. Comparison to observed storms and further discussion

In light of these results, we would be remiss if we did not inquire as to the radial distributions of diabatic heating and inertial stability in real storms. In particular, does the location of the radius of maximum wind relative to the heating really play a prominent role in controlling intensification rates in observed storms? Seeking to answer this question, we turn our attention to observational studies that have shed some light on this issue.

a. Location of diabatic heating relative to the radius of maximum wind in observed storms

Shea and Gray (1973) conducted a landmark study in which they examined 533 radial flight legs from Atlantic hurricanes over a 13-yr period. They characterized the radius of maximum wind as the boundary between two dynamically disparate regions of the storm. Outside the radius of maximum winds, convergence and high winds dominate, whereas high winds, high vorticity, and subsidence are found inside the radius of maximum winds. At low levels, air flowing in toward the radius of maximum wind meets air flowing outwards from the eye, forcing a strong updraft at or near the radius of maximum wind. Thus, in the overwhelming majority of cases, the radius of maximum wind occurs *within* the eyewall cloud.[4] In fact, on average, the radius of maximum wind was located 8–10 km outward from the inner edge of the eyewall (as observed by aircraft radar). Jorgensen (1984) made additional observations of mature hurricanes that possessed contracting eyewalls; his results show that the maximum convective-scale updrafts (which correspond to the maximum diabatic heating) are typically located between 1 and 6 km inward from the radius of maximum wind. These observations indicate that significant diabatic heating normally occurs within the high-inertial-stability region of most storms. Thus, the typical tropical cyclone structure clearly supports intensification, but the more interesting question still remains: what controls how rapidly a storm will intensify?

It is not a trivial matter to resolve the radial distribution of diabatic heating in a tropical cyclone. Several past studies have used satellite-based passive microwave radiometer data or aircraft to examine the relationship between inner-core diabatic heating and intensity change. Some general findings of those studies are summarized here. (i) As a storm develops and intensifies from a disturbance to the hurricane stage, inner-core diabatic heating tends to increase and concentrate toward the center (Adler and Rodgers 1977; Lonfat et al. 2004). (ii) Episodes of enhanced heating seem to precede periods of intensification, with perhaps a lag of a day or two (Rodgers and Adler 1981; Steranka et al. 1986; Rao and MacArthur 1994). (iii) The storm tends to become more responsive to increases in inner-core diabatic heating as the intensity increases (Rodgers et al. 1998); hurricanes may need less of an increase in heating to intensify as compared with tropical storms (Rodgers et al. 1994). (iv) In the mature stage, however, Marks (1985) observed no relationship between Hurricane Allen's (1980) intensity changes and inner-core diabatic heating over a 5-day period. Increases in latent heat seemed to be related to areal increases in rainfall caused by rainband activity or the presence of multiple eyewalls.

Most of the above studies share several common weaknesses. First of all, it is difficult to separate the intensification response due to increased inner-core diabatic heating from the general tendency of the diabatic heating to concentrate near the center as the storm intensifies. Additionally, the early satellite-based estimates of diabatic heating could not adequately resolve the radial distribution of diabatic heating. Finally, these studies did not include any information on the distribution of heating relative to the radius of maximum winds.

One study has overcome some of these limitations. Corbosiero et al. (2005; see their Fig. 6) have performed a detailed investigation of Hurricane Elena (1985) data during a 28-h period when it was well observed by both ground-based radar and aircraft. These data show that during Elena's period of most rapid intensification, the radius of maximum wind contracted to approximately 30 km and the inner edge of the eyewall convection remained at approximately 20 km, while there appeared to be periods of intense convection in the region between 20 and 30 km. According to the analysis presented here, the portion of the diabatic heating that occurred between 20 and 30 km was most responsible for the intensification of Elena. Because this is just one case, and the intensification rate appears to be constant during this period (as indicated from the best track,

[4] In a small number of cases, the radius of maximum wind was found *inside* the eye. This suggests that diabatic heating associated with the eyewall updraft may occur entirely outside of the high-inertial-stability region. Our Fig. 2 suggests that any such distribution of heating will be very inefficient at intensifying the storm.

which only gives intensity values every 6 h), it is difficult to tell whether the concentration of diabatic heating within the radius of maximum winds actually affected Elena's intensification rate.

Returning to the study of Shea and Gray, their Fig. 18 plots the difference between the radius of maximum wind and the inner eye radius as a function of intensity. This distance measures how far within the cloud area the radius of maximum wind resides and can be thought of as a crude proxy for the amount of efficient diabatic heating. According to the figure, storms near minimal hurricane intensity exhibit a wide variation in this quantity (with the radius of maximum wind sometimes occurring near the inner cloud edge but in other cases lying more than 40 km outward from the inner cloud edge). Their figure bolsters the view that the proportion of diabatic heating located within the radius of maximum decreases as a storm intensifies. But clearly an observational challenge remains to continue to document, for a broad set of storms with widely varying intensification rates, the relation between the radius of maximum wind and the inner edge of eyewall convection.

b. *Effects of eye formation and contraction*

Because the formation of an eye[5] must necessarily remove some of the diabatic heating from the high-inertial-stability region of a storm, Schubert and Hack (1982) viewed eye formation as a stabilizing factor that prevents runaway intensification. On the other hand, observations suggest that storms often intensify most rapidly during or immediately following the formation of an eye (Mundell 1990). The argument for eye formation as a stabilizer to storm intensification can be summarized thus: Convective heating in the consolidating eyewall forces central axial subsidence, increasing static stability in the nascent eye. At the same time, the increased inertial stability associated with the intensifying swirling flow of the developing eyewall acts as a barrier to moist air flowing toward the center. With the moisture-rich low-level source air becoming ''locked out'' from the center, and any remaining convection being ''locked down'' by the increasing static stability, diabatic heating is removed from the high-inertial-stability region and an eye appears. All things being equal, this change in the radial distribution of heating should decrease a storm's overall heating efficiency, thereby retarding the intensification rate.

[5] The dynamical mechanisms responsible for eye formation are not discussed here, but most surely involve the remarkable property for the boundary layer Ekman pumping to maximize at a finite radius rather than at $r = 0$ (see Eliassen and Lystad 1977).

However, all other things are clearly not equal when an intensifying storm forms an eye. While it is true that the development of an eye must necessarily remove diabatic heating from the center, significant heating still occurs between the inner edge of the eyewall and the radius of maximum winds. During intensification both the radius of maximum winds and the inner edge of diabatic heating tend to move inward in accordance with the convective ring hypothesis discussed by Willoughby et al. (1982, 1984) and Willoughby (1990). Although the area of efficient heating may shrink in physical space, when viewed in potential radius coordinates, the ''dynamic size'' of the heated area may actually increase if the angular momentum surfaces move inward faster than the edge of the convective heating (Schubert and Hack 1983). Since the reduction in the radius of maximum wind and the increase in tangential winds both act to dramatically shrink the local Rossby length in the eyewall, *the intensification rate of a storm increases as its spatial scale shrinks and its intensity increases*. This has been shown recently by Pendergrass and Willoughby (2009), who used a more general framework to solve the Sawyer–Eliassen equation for a piecewise-continuous balanced mean vortex that includes a realistic vertical shear. Their realistic vortex case (their Fig. 9a) shows that the tangential wind tendency experiences a rapid increase as the maximum wind crosses the 30–35 m s^{-1} threshold. As Shapiro and Willoughby (1982) note, this is the threshold at which a tropical cyclone tends to form an eye.

In addition to the effects of spatial scale and intensity, the eyewall heating rate likely increases as the eyewall organization improves. Thus, the storm concentrates its diabatic heating in the area where the inertial stability is most rapidly increasing. As a result, continued increases in the efficiency of the eyewall heating can offset the losses in efficiency that result from removal of diabatic heating from the eye. Neglecting other factors, it seems likely that the net effect of eye formation is to increase the storm's intensification rate.

c. *Maturation of the warm core and approach to a steady state*

As the storm continues to intensify and warm air overspreads the inner core, several factors begin to act against further intensification. First of all, rising air parcels require increasing amounts of energy to overcome the warmer temperatures aloft; this tends to hinder deep upright convection (Ooyama 1969). Second, the increased static stability imposes an additional source of resistance to the secondary circulation. This tends to reduce the convergence of moisture and angular momentum into the inner core. Both of these factors decrease the inner-core

heating, countering the increased efficiency gains that occur because of eye contraction. Eventually, the maturation of the warm core should cause the storm to approach a steady state. These negative influences may be minimized if the storm is able to concentrate the warming as high as possible and as close to the center as possible (Mundell 1990). The details of the vertical distribution of the warm core response depend on the influence of baroclinity, an effect which is not included in our mathematical framework but which is likely very important [van Delden (1989) suggests that baroclinity enhances deepening rates when the maximum winds speed exceeds 30 m s^{-1}]. Eventually, the region of efficient heating in the eyewall collapses to a small finite area through which only a certain amount of mass flux can occur to drive diabatic heating. These ideas suggest that the ultimate intensity achieved by the storm may depend in part on the vertical and spatial distribution of the warm core and on the amount of diabatic heating that remains in the efficient region of the eyewall. This ''dynamical limit'' view of intensification is surely not the whole picture, but it may offer further avenues of investigation by models of intermediate complexity.

d. Analogy to stratospheric sudden warming

Dr. T. Dunkerton (2009, personal communication) has pointed out the existence of a useful analogy between the hurricane problem considered here and the stratospheric sudden warming problem considered by Matsuno and Nakamura (1979) and Dunkerton (1989). In the idealized hurricane problem the secondary circulation is driven by a ''vertical delta surface'' of diabatic heating, whereas in the idealized stratospheric sudden warming problem the Lagrangian mean circulation is driven by an Eliassen–Palm flux convergence that is singular at a given height (i.e., by a ''horizontal delta surface'' that provides a ''zonal force'' that drives a transformed Eulerian mean circulation). An important difference between the two problems is that quasigeostrophic theory is a useful dynamical framework for studying stratospheric sudden warming, but the gradient balanced vortex model is necessary for the highly curved, large-Rossby-number flows in hurricanes.

8. Concluding remarks

It has been known for several decades that one of the necessary conditions for hurricane development is that diabatic heating occur in the region of high inertial stability. Compared to past studies, the present study is unique in that it has analytically solved for the temperature tendency associated with a vertical delta surface of diabatic heating in a vortex with a simple radial dependence of inertial stability. The solutions emphasize the fact that diabatic heating in the low-inertial-stability region outside the radius of maximum wind is inefficient at generating a warm core, no matter how large the current storm intensity. In contrast, diabatic heating in the high-inertial-stability region inside the radius of maximum wind is efficient at generating a localized temperature tendency, and this efficiency increases dramatically with storm intensity. In other words, the present results emphasize that the vortex intensification rate depends *critically* on how much of the heating is occurring inside the radius of maximum wind. However, when a tropical cyclone reaches a minimum surface pressure of approximately 985 hPa and a maximum tangential wind of approximately 35 m s^{-1}, an eye forms, and diabatic heating becomes at least partially locked out of the high-inertial-stability region. Thus, it can be argued that storms that continue rapid intensification after eye formation are those in which at least some of the diabatic heating persists in the high-inertial-stability region inside the radius of maximum wind. Our results suggest that the shrinking effect on the local Rossby length due to the decreasing spatial scale and increasing tangential winds compensates for the loss of efficiency due to eye formation.

In closing, it is interesting to note that we have derived the Green's functions for the transverse circulation Eq. (2.11) and the geopotential tendency Eq. (2.21) in the special case of a resting atmosphere and the special case of a height-independent Rankine-like vortex. In these special cases the differential operators in (2.11) and (2.21) simplify considerably. Obviously, it would be useful to obtain the corresponding Green's functions for a general baroclinic vortex. Such baroclinic Green's functions would aid in understanding the role of eyewall slope and in understanding how a steady state is approached as the ratio of $\dot{\theta}$ to P becomes constant along each absolute angular momentum surface. One approach to this more difficult baroclinic problem is to transform (2.11) and (2.21) from (r, z) coordinates to either (R, z) coordinates (where $\frac{1}{2} f R^2 = m$) or (r, θ) coordinates. In both cases, the operators on the left-hand sides of (2.11) and (2.21) are considerably simplified, so that simple analytical solutions can be found.

Acknowledgments. We thank Chris Rozoff, Tim Dunkerton, Mary Haley, Paul Ciesielski, Mark DeMaria, Levi Silvers, Eric Hendricks, Kevin Mallen, Brian McNoldy, Kate Musgrave, Rick Taft, Ed Zipser, and an anonymous reviewer for their advice and helpful comments. This research was supported by NASA/TCSP Grant NNG06GA54G and NSF Grant ATM-0332197.

REFERENCES

Abramowitz, M., and I. A. Stegun, 2006: *Handbook of Mathematical Functions*. Dover, 1046 pp.

Adler, R. F., and E. B. Rodgers, 1977: Satellite-observed latent heat release in a tropical cyclone. *Mon. Wea. Rev.,* **105,** 956–963.

Corbosiero, K. L., J. Molinari, and M. L. Black, 2005: The structure and evolution of Hurricane Elena (1985). Part I: Symmetric intensification. *Mon. Wea. Rev.,* **133,** 2905–2921.

Dunkerton, T. J., 1989: Body force circulations in a compressible atmosphere: Key concepts. *Pure Appl. Geophys.,* **130,** 243–262.

Eliassen, A., 1951: Slow thermally or frictionally controlled meridional circulation in a circular vortex. *Astrophys. Norv.,* **5,** 19–60.

——, and M. Lystad, 1977: The Ekman layer of a circular vortex: A numerical and theoretical study. *Geophys. Norv.,* **31,** 1–16.

Gill, A. E., 1982: *Atmosphere–Ocean Dynamics*. International Geophysics Series, Vol. 30, Academic Press, 662 pp.

Hack, J. J., and W. H. Schubert, 1986: Nonlinear response of atmospheric vortices to heating by organized cumulus convection. *J. Atmos. Sci.,* **43,** 1559–1573.

Hausman, S. A., K. V. Ooyama, and W. H. Schubert, 2006: Potential vorticity structure of simulated hurricanes. *J. Atmos. Sci.,* **63,** 87–108.

Haynes, P. H., and T. G. Shepherd, 1989: The importance of surface pressure changes in the response of the atmosphere to zonally-symmetric thermal and mechanical forcing. *Quart. J. Roy. Meteor. Soc.,* **115,** 1181–1208.

Holland, G. J., and R. T. Merrill, 1984: On the dynamics of tropical cyclone structural changes. *Quart. J. Roy. Meteor. Soc.,* **110,** 723–745.

Jorgensen, D. P., 1984: Mesoscale and convective-scale characteristics of mature hurricanes. Part I: General observations by research aircraft. *J. Atmos. Sci.,* **41,** 1268–1286.

Knaff, J. A., J. P. Kossin, and M. DeMaria, 2003: Annular hurricanes. *Wea. Forecasting,* **18,** 204–223.

Lonfat, M., F. D. Marks Jr., and S. S. Chen, 2004: Precipitation distribution in tropical cyclones using the Tropical Rainfall Measuring Mission TRMM microwave imager: A global perspective. *Mon. Wea. Rev.,* **132,** 1645–1660.

Mallen, K. J., M. T. Montgomery, and B. Wang, 2005: Reexamining the near-core radial structure of the tropical cyclone primary circulation: Implications for vortex resiliency. *J. Atmos. Sci.,* **62,** 408–425.

Marks, F. D., Jr., 1985: Evolution of the structure of precipitation in Hurricane Allen. *Mon. Wea. Rev.,* **113,** 909–930.

Matsuno, T., and K. Nakamura, 1979: The Eulerian- and Lagrangian-mean meridional circulations in the stratosphere at the time of a sudden warming. *J. Atmos. Sci.,* **36,** 640–654.

Mundell, D. B., 1990: Prediction of tropical cyclone rapid intensification. M.S. thesis, Dept. of Atmospheric Science, Colorado State University, 186 pp.

Nolan, D. S., Y. Moon, and D. P. Stern, 2007: Tropical cyclone intensification from asymmetric convection: Energetics and efficiency. *J. Atmos. Sci.,* **64,** 3377–3405.

Ooyama, K., 1969: Numerical simulation of the life cycle of tropical cyclones. *J. Atmos. Sci.,* **26,** 3–40.

Pendergrass, A. G., and H. E. Willoughby, 2009: Diabatically induced secondary flows in tropical cyclones. Part I: Quasi-steady forcing. *Mon. Wea. Rev.,* **137,** 805–821.

Rao, G. V., and P. D. MacArthur, 1994: The SSM/I estimated rainfall amounts of tropical cyclones and their potential in predicting the cyclone intensity changes. *Mon. Wea. Rev.,* **122,** 1568–1574.

Rodgers, E. B., and R. F. Adler, 1981: Tropical cyclone rainfall characteristics as determined from a satellite passive microwave radiometer. *Mon. Wea. Rev.,* **109,** 506–521.

——, S. Chang, and H. F. Pierce, 1994: A satellite observational and numerical study of precipitation characteristics in Western North Atlantic tropical cyclones. *J. Appl. Meteor.,* **33,** 129–139.

——, W. S. Olson, V. M. Karyampudi, and H. F. Pierce, 1998: Satellite-derived latent heating distribution and environmental influences in Hurricane Opal (1995). *Mon. Wea. Rev.,* **126,** 1229–1247.

——, W. Olson, J. Halverson, J. Simpson, and H. Pierce, 2000: Environmental forcing of Supertyphoon Paka's (1997) latent heat structure. *J. Appl. Meteor.,* **39,** 1983–2006.

Schubert, W. H., and J. J. Hack, 1982: Inertial stability and tropical cyclone development. *J. Atmos. Sci.,* **39,** 1687–1697.

——, and ——, 1983: Transformed Eliassen balanced vortex model. *J. Atmos. Sci.,* **40,** 1571–1583.

——, ——, P. L. Silva Dias, and S. R. Fulton, 1980: Geostrophic adjustment in an axisymmetric vortex. *J. Atmos. Sci.,* **37,** 1464–1484.

——, C. M. Rozoff, J. L. Vigh, B. D. McNoldy, and J. P. Kossin, 2007: On the distribution of subsidence in the hurricane eye. *Quart. J. Roy. Meteor. Soc.,* **133,** 595–605, doi:10.1002/qj.49.

Shapiro, L. J., and H. E. Willoughby, 1982: The response of balanced hurricanes to local sources of heat and momentum. *J. Atmos. Sci.,* **39,** 378–394.

Shea, D. J., and W. M. Gray, 1973: The hurricane's inner core region. I. Symmetric and asymmetric structure. *J. Atmos. Sci.,* **30,** 1544–1564.

Steranka, J., E. B. Rodgers, and R. C. Gentry, 1986: The relationship between satellite measured convective bursts and tropical cyclone intensification. *Mon. Wea. Rev.,* **114,** 1539–1546.

van Delden, A., 1989: On the deepening and filling of balanced cyclones by diabatic heating. *Meteor. Atmos. Phys.,* **41,** 127–145.

Wang, Y., 2008: Structure and formation of an annular hurricane simulated in a fully compressible, nonhydrostatic model—TCM4. *J. Atmos. Sci.,* **65,** 1505–1527.

Willoughby, H. E., 1979: Forced secondary circulations in hurricanes. *J. Geophys. Res.,* **84,** 3173–3183.

——, 1990: Temporal changes of the primary circulation in tropical cyclones. *J. Atmos. Sci.,* **47,** 242–264.

——, J. A. Clos, and M. G. Shoreibah, 1982: Concentric eye walls, secondary wind maxima, and the evolution of the hurricane vortex. *J. Atmos. Sci.,* **39,** 395–411.

——, H.-L. Jin, S. J. Lord, and J. M. Piotrowicz, 1984: Hurricane structure and evolution as simulated by an axisymmetric, nonhydrostatic numerical model. *J. Atmos. Sci.,* **41,** 1169–1186.

Wirth, V., and T. J. Dunkerton, 2006: A unified perspective on the dynamics of axisymmetric hurricanes and monsoons. *J. Atmos. Sci.,* **63,** 2529–2547.